

Nonlinear combining and compression in multicore fibersI. S. Chekhovskoy,^{1,2} A. M. Rubenchik,³ O. V. Shtyrina,^{1,2} M. P. Fedoruk,^{1,2} and S. K. Turitsyn^{1,4}¹*Novosibirsk State University, Novosibirsk 630090, Russia*²*Institute of Computational Technologies SB RAS, Novosibirsk 630090, Russia*³*Lawrence Livermore National Laboratory, Livermore, California 94550, USA*⁴*Aston Institute of Photonic Technologies, Aston University, Birmingham B4 7ET, United Kingdom*

(Received 23 June 2016; published 25 October 2016)

We demonstrate numerically light-pulse combining and pulse compression using wave-collapse (self-focusing) energy-localization dynamics in a continuous-discrete nonlinear system, as implemented in a multicore fiber (MCF) using one-dimensional (1D) and 2D core distribution designs. Large-scale numerical simulations were performed to determine the conditions of the most efficient coherent combining and compression of pulses injected into the considered MCFs. We demonstrate the possibility of combining in a single core 90% of the total energy of pulses initially injected into all cores of a 7-core MCF with a hexagonal lattice. A pulse compression factor of about 720 can be obtained with a 19-core ring MCF.

DOI: [10.1103/PhysRevA.94.043848](https://doi.org/10.1103/PhysRevA.94.043848)**I. INTRODUCTION**

The technology of optical multicore fibers (MCFs) is one of the possible methods of implementing spatial-division multiplexing (SDM) for future high-capacity optical communications (see [1–9]). A brute-force solution of the ever-growing capacity problem is to deploy multiple communication systems over parallel fibers in order to meet demand. However, the use of multiple systems over parallel fibers will lead to linearly scaled (with growing capacity) transmission costs and power consumption. The SDM technology might potentially enable a substantial reduction in cost per bit and improved energy efficiency. At the moment, however, SDM technology is in the research stage and major research activities worldwide are exploring and testing various MCF designs and this potentially disruptive new platform. In MCFs the optical pathways are defined by an array of physically distinct single-mode cores. In conventional optical communications, the nonlinear effects that occur during signal propagation in a fiber due to the proximity of other data-transmission channels are typically undesirable. An obvious approach to limiting cross-talk between spatial channels is to keep the fiber cores well spaced. Laboratory experiments demonstrate the feasibility of MCF technology for Pb/s fiber transmission [10].

The MCFs can also be used for very different, high-power applications [11]. At high signal power and coupling among cores, existing MCFs can be also considered as nonlinear discrete physical systems, interesting both for fundamental science [12,13] and for various potential practical applications as nonlinear photonic devices [14,15]. With a large number of cores, the continuous limit of discrete models in the form of the well-known nonlinear Schrödinger (NLS) equations can be used for a qualitative understanding of the system evolution. In particular, for propagation in MCFs with the so-called anomalous dispersion, the two- and three-dimensional NLS equations describe the well-known effects of self-focusing and wave collapse. Specifically, pulse compression and concentration of the energy in a few fibers are expected (see [16] and references therein).

When the energy is concentrated in a single core, the problem becomes effectively one-dimensional and the collapse

stops. Hence, the discreteness must limit the the combining and compression. The idea to use the collapse for pulse compression in fiber arrays was proposed more than 20 years ago [16], but to build the fiber arrays is an technological challenge. A multicore fiber is an example of a fiber array with a specific distribution of relatively low total number of cores in which the proposed ideas can be implemented. This type of nonlinear combining is substantially different from currently popular schemes of linear beam combining [17] and can be advantageous for some other energy-transfer and -delivery applications.

In this paper we focus on a theoretical study of the key underlying models and their mathematical properties. We consider two types of MCF. In the first, the cores are placed as a ring in the fiber cross section with each core interacting with two neighbors only (see Fig. 1). In this case, the continuous model is the two-dimensional (2D) nonlinear Schrödinger equation.

As a second example, we examine hexagonal or square positioning of the cores (2D core distribution, as shown in Fig. 2) with each core interacting with several (more than two, compared to the first case) neighbors, resulting in a stronger nonlinear interaction. The continuous model in this situation is the 3D NLS equation (NLSE). The evolution of NLSE collapsing solutions, in both 2D and 3D, has been studied in detail (see, for example, the review [18]). Using these classical results, we can obtain insight into the optimization of the energy-localization process.

The existence of such regimes was demonstrated in our previous paper [19]. There it was shown that pulses initially injected into all cores of a MCF were combined into a small number of cores with simultaneous pulse compression. In this paper, we evaluate through numerical modeling optimal conditions for nonlinear pulse combining and compression in multicore fibers. We study the process for MCF with different core numbers which corresponds to an increase of collapse range. We found a qualitative difference in compression and combining for the ring and 2D configurations (hexagonal and square lattices).

We demonstrate that the conditions for optimal combining and compression are substantially different. In the 7-core ring

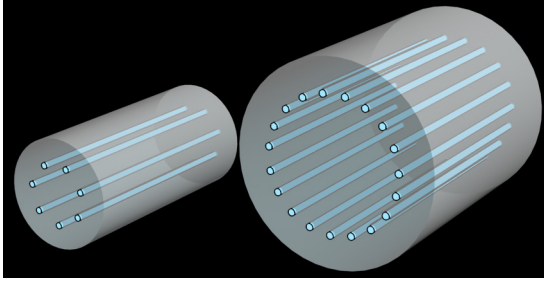


FIG. 1. Schematic depiction of the considered MCF waveguide with 7 (left) and 19 (right) cores arranged in a circle.

MCF we demonstrate a combining of 83.5% of energy into a single core and pulse compression over 300 times. In the 19-core ring MCF we find regimes with 80% energy combining and 720 times compression. Numerical modeling established that a 7-core hexagonal MCF allowed us to combine 91.6% of energy and to compress an optical pulse up to 256 times. In the case of a 19-core hexagonal fiber, we find regimes providing 80.9% energy combining and compression with a factor of 250.

We demonstrate that the 2D distribution of the cores across the MCFs (see Fig. 2) increases the nonlinear interaction between the channels, but this does not result in improvement of the compression and combining efficiency compared to ring configurations. However, 2D placement of the cores greatly reduces the combining and compression length which can be useful and is an important feature for practical device design. Moreover, the combining and compression in a 2D MCF is more robust and insensitive to variation of the initial parameters. The analysis of the NLSE continuous limit helps us to understand these results.

Finally, we summarize the results of the optimization for the combining and compression, and we present the optimal (within the considered schemes) MCF design. We also briefly discuss the possible practical devices and their parameters.

II. BASIC EQUATIONS: SELF-FOCUSING AND COLLAPSE IN 2D AND 3D

The electromagnetic field of optical pulses propagating along MCF with 1D core distribution can be well approximated by a superposition of modes,

$$E(x, y, z, t) = \sum_k A_k(z, t) F_k(x - x_k, y - y_k) e^{i(\beta_k z - \omega t)} + \text{c.c.}, \quad (1)$$

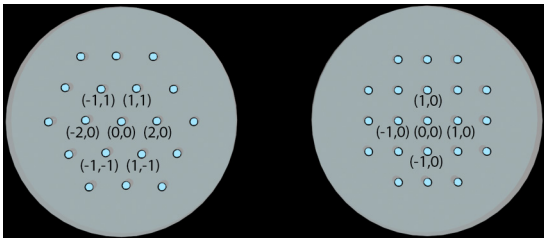


FIG. 2. Schematic depiction of the considered multicore fiber with hexagonal and square geometry and 2D numbering of cores.

where F gives the spatial mode structure and A_k is the complex envelope of the electromagnetic field in core number k . In the limit of a weak-coupling approximation one can derive a system of equations for the envelopes A_k , i.e., the continuous-discrete nonlinear Schrödinger equation [15],

$$i \frac{\partial A_k}{\partial z} = \frac{\beta_2^k}{2} \frac{\partial^2 A_k}{\partial t^2} - \gamma_k |A_k|^2 A_k - \sum_{m=1, m \neq k}^N C_{km} A_m, \quad (2)$$

where $k = 1, \dots, N$, β_2^k is the group-velocity dispersion parameter for the mode k , γ_k is the Kerr parameter, and the quantities C_{km} are the coupling coefficients between the cores. In such approximation mutual nonlinear interactions are several orders of magnitude smaller in comparison with self-nonlinearity, so they can be neglected [15,20,21].

The system (2) can be simplified for the case of identical cores as discussed in [13]. Consider first the ring core geometry (Fig. 1). Taking into account the interaction between nearest neighbors only, we can simplify the analysis with the assumption

$$C_{k,k+1} = C > 0 \quad (3)$$

and neglect all other coupling terms. We consider $\beta_2^k = \beta_2 < 0$, $\gamma_k = \gamma$ ($k = 1, \dots, N$).

It is convenient to introduce normalized variables, $A_k = \exp(i2z') \sqrt{C/\gamma} U_k$, where $z' = z/L$, $L = 1/C$, $t' = t/T$, $T^2 = -\beta_2/(2C)$. The dimensionless equations (omitting the primes) read

$$i \frac{\partial U_k}{\partial z} = -\frac{\partial^2 U_k}{\partial t^2} - (U_{k+1} - 2U_k + U_{k-1}) - |U_k|^2 U_k. \quad (4)$$

In the case of a 2D core distribution we have the system for the envelopes $A_{n,m}$ [22],

$$i \frac{\partial A_{n,m}}{\partial z} = \frac{\beta_2}{2} \frac{\partial^2 A_{n,m}}{\partial t^2} - \sum_{(k,l) \neq (n,m)} C_{n,m,k,l} A_{k,l} - \gamma |A_{n,m}|^2 A_{n,m}. \quad (5)$$

Consider two different geometries, the square and hexagonal lattices (Fig. 2). We introduce normalized envelopes $A_{n,m} = \exp(i4z') \sqrt{C/\gamma} U_{n,m}$ for the square geometry and $A_{n,m} = \exp(i6z') \sqrt{C/\gamma} U_{n,m}$ for hexagonal geometry, where C is the same for all the neighboring core coupling coefficients (other couplings may be neglected) and dimensionless variables $z' = z/L$, $L = 1/C$, and $t' = t/T$, $T^2 = -\beta_2/(2C)$, the same as for the ring geometry. Finally, omitting the primes, the system of NLSE takes the form [22]

$$i \frac{\partial U_{n,m}}{\partial z} + \frac{\partial^2 U_{n,m}}{\partial t^2} + (\underline{CU})_{n,m} + |U_{n,m}|^2 U_{n,m} = 0, \quad (6)$$

where $(\underline{CU})_{n,m}$ is the linear coupling profile at site (n,m) . For the square and hexagonal core configurations, the combination $(\underline{CU})_{n,m}$ is given by expression

$$\begin{aligned} (\underline{CU})_{n,m}^{\text{sqr.}} &= U_{n-1,m} + U_{n+1,m} + U_{n,m-1} + U_{n,m+1} - 4U_{n,m}, \\ (\underline{CU})_{n,m}^{\text{hex.}} &= U_{n-1,m-1} + U_{n+1,m-1} + U_{n-2,m} \\ &\quad + U_{n+2,m} + U_{n-1,m+1} + U_{n+1,m+1} - 6U_{n,m}. \end{aligned} \quad (7)$$

The continuous-discrete NLSEs (4) and (6) conserve the total energy (normalized by C/γ),

$$(1D) \quad E = \sum_{k=1}^N \int_{-\infty}^{\infty} |U_k(z,t)|^2 dt,$$

$$(2D) \quad E = \sum_{n,m} \int_{-\infty}^{\infty} |U_{n,m}(z,t)|^2 dt, \quad (8)$$

and Hamiltonian

$$(1D)$$

$$H = \sum_{k=1}^N \int_{-\infty}^{\infty} \left[\left| \frac{\partial U_k}{\partial t} \right|^2 + |U_k - U_{k-1}|^2 - \frac{|U_k|^4}{2} \right] dt,$$

$$(2D)$$

$$H = \sum_{n,m} \int_{-\infty}^{\infty} \left[\left| \frac{\partial U_{n,m}}{\partial t} \right|^2 - (CU)_{n,m} U_{n,m}^* - \frac{|U_{n,m}|^4}{2} \right] dt, \quad (9)$$

and the master equations have the Hamiltonian structure:

$$i \frac{\partial U_{n,m}}{\partial z} = \frac{\delta H}{\delta U_{n,m}^*}. \quad (10)$$

The system (4) with a large number of cores and smooth intensity distribution that experiences only small changes between neighboring cores for the ring geometry (Fig. 1) is equivalent to the continuous 2D NLSE for $U(k,t,z)$, considering the index k as a continuous variable,

$$i \frac{\partial U}{\partial z} + \frac{\partial^2 U}{\partial t^2} + \frac{\partial^2 U}{\partial k^2} + |U|^2 U = 0, \quad (11)$$

with Hamiltonian

$$H = \int_{-\infty}^{\infty} \left[\left| \frac{\partial U}{\partial t} \right|^2 + \left| \frac{\partial U}{\partial k} \right|^2 - \frac{|U|^4}{2} \right] dt. \quad (12)$$

Equation (11) is equivalent to the NLSE that describes the self-focusing of light in various nonlinear media. The continuous analog can be used for insight in discrete system evolution.

In the conventional theory of self-focusing governed by the NLSE, the initial wave distribution collapses into singularity when the Hamiltonian H is negative or when the beam power exceeds the critical value P_{cr} . This value depends on the beam shape and is minimal for the Townes mode. In our case, the role of power is played by the total energy injected into the MCF $E = \int dt dn |U_n|^2$. When the input energy exceeds the critical value E_0 [for the Townes beam, $E_0 = E_{cr} = 4\pi$, in terms of the dimensional variables $E_{cr} = 4\pi \sqrt{-C\beta_2/(2\gamma^2)}$], making $H < 0$, the intensity distribution is self-compressed over k and t . We can expect that the injected MCF pulses distributed over the cores with smooth maxima will be focused into a few cores around the maxima with simultaneous pulse compression. When the energy is concentrated into a few cores the discreteness of the cores arrests further compression. When the input energy $E \gg 4\pi$, the distribution breaks into a few collapsing clusters with $E \approx 4\pi$ (similar to filamentation in the continuum limit). In every cluster the compression and combining takes place, but the location of the peaks is difficult to predict and this situation

is not practical for the goals of beam combining or pulse compression.

The continuous version of the continuous-discrete 3D NSLE (Fig. 2) takes the form

$$i \frac{\partial U}{\partial z} + \frac{\partial^2 U}{\partial t^2} + \frac{\partial^2 U}{\partial k^2} + \frac{\partial^2 U}{\partial l^2} + |U|^2 U = 0 \quad (13)$$

for $U(z,t,k,l)$, where the spatial variables k and l take the values of a certain bounded domain S [e.g., $S = \{(k,l) : k^2 + l^2 < R^2\}$ for a circle of radius R]. The Hamiltonian in this case has the following form:

$$H = \int_{-\infty}^{\infty} \int_S \left[\left| \frac{\partial U}{\partial t} \right|^2 + \left| \frac{\partial U}{\partial k} \right|^2 + \left| \frac{\partial U}{\partial l} \right|^2 - \frac{|U|^4}{2} \right] dk dl dt. \quad (14)$$

An increase in the number of neighbors enhances the nonlinear interaction and makes collapse possible even for positive values of H [23]. In this case we can expect that the injected MCF pulses will be focused into a few central cores with simultaneous pulse compression. Nonlinear systems described by Eq. (13) have stronger collapsing features, and a MCF with 2D configuration of cores could demonstrate better compression results, which will be shown later. In the 3D situation, the collapse is ‘‘weak’’ (see definitions in [23]) and the energy involved in the compression processes decreases [18]. In this case, the optimal compression and combining is reached in a transient regime and the choice of parameters is not universal. We will present the results of the modeling of compression and combining in both situations and will examine the selection of the optimal parameters.

III. 2D COMPRESSION AND ENERGY COMBINING IN 7-CORE AND 19-CORE RING MCFs

First we consider pulse evolution in MCFs with the ring design shown in Fig. 1. The 7-core and 19-core MCFs with the cores arranged in a circle are considered for comparing with 7- and 19-core hexagonal MCFs. All simulations were based on the model (4). The analysis of pulse compression and combining in a MCF with 1D location of the cores was carried out for the initial conditions given by the same Gaussian pulses in each core,

$$U_k(0,t) = \sqrt{P} \exp\left(-\frac{t^2}{2\tau^2}\right) \left[1 + M \cos\left(\frac{2\pi k}{N}\right)\right], \quad (15)$$

where M is the modulation coefficient, and $k = 1, \dots, N$. The modulation $M \cos(2\pi k/N)$ produces the smooth initial intensity modulation with a maximum in the designated core. This modulation accelerates the compression and, most importantly, makes it less sensitive to the perturbation of the initial parameters. On the other hand, the perturbation must be small enough for the efficient utilization of each core ($M \ll 1$). Recently [19], we demonstrated effective compression and combining in this situation. Here we present the optimal parameters for the most efficient system performance. Based on the results of the previous study [19], we set $M = 0.3$.

We perform simulation of light-pulse propagation initially distributed according to Eq. (15) aiming at the optimization of pulse compression and energy combining. The dependencies of the basic compression parameters are obtained for the range of parameters $P \in [0.31; 1000]$, $\tau \in [0.05; 60]$ for the 7-core MCF and $P \in [0.05; 1000]$, $\tau \in [0.05; 230]$ for the 19-core MCF. The numerical solution of Eqs. (4) was performed by the split-step Fourier method with the Padé approximation with scaling and squaring for the matrix exponential (see [24,25]).

The range of values of the initial pulse parameters P and τ was discretized by 250×250 nodes. For each parameter pair (P, τ) of the grid, the simulation of the dynamics of optical pulses with the form (15) injected into every core of the appropriate MCF was made. We tracked the first peak power maximum of the propagating pulse to get the compression or energy conversion at the minimum possible distance along the fiber. In what follows we call such a distance an ‘‘optimal’’ one. Moreover, we took into account only those maxima at which peak power is increased by more than $0.2N$ times, where N is the number of cores ($N > 5$). This approach was applied to cut off the situations when the peak power maximum is observed without the pulse compression. The value $0.2N$ was chosen empirically. When the energy E is comparable with E_{cr} , the particular initial distribution is not optimal and it can have a few oscillations before the collapse (here, sharp energy localization to few cores). In this situation, even when strong compression and combining takes place, the position of peaks is sensitive to the initial variations of the power and pulse durations and, for the purpose of this study, we consider the situation as not practical. The above procedure eliminates this type of dynamics. The general further ‘‘turbulent’’ evolution after peak compression (combining) is complex (see, e.g., [26]) and beyond the frame of this paper. It is worth noting that in the general case the parameters for the optimal temporal pulse compression and maximum energy combining in a single core are different, and the distances along the fiber z_0 of maximum compression and combining are also varying in modeling.

An initial demonstration of the effect for the ring configuration was discussed in [19]. Here we present a more detailed study of the parameter space and evaluation of the optimal input signal characteristics for compression and combining.

The maps of combining and compression performance for the 7-core ring MCF are presented in Fig. 3. In Fig. 3(a) we see the coherent effective beam combining. For the optimal choice of parameters, 83.5% of the initial energy is combined in one core at the distance 10.36 (in the dimensionless variable z). The combined pulse is smooth, and the side satellite peaks have an intensity of 4% of the peak intensity. The total energy in the wings is about 1.9%. Note that the region of the maximal combining lies close to the line $H = 0$. The map of the compression efficiency is quite different. The blue area denotes pairs of parameters P and τ , for which there is no pulse compression or the initial pulses (15) break into clusters as a result of the modulation instability. It is interesting that isolines of pulse compression factor in Fig. 3(b) correlate with isolines of the ratio of the dispersion length $L_D = \tau^2/|\beta_2|$ and the nonlinear length $L_{NL} = 1/(\gamma P)$. The zone of optimal compression is the stripe narrowing toward high total energies and is confined by the level $L_D/L_{NL} \approx 3000$. If $L_D/L_{NL} > 3000$, a large nonlinearity destroys a smooth pulse shape before

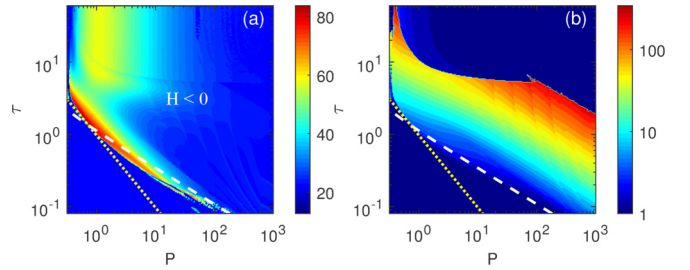


FIG. 3. Dependence of the percentage of total energy E combined in the core with pulse compression (a) and the pulse-width compression factor in the logarithmic scale (b) on the initial pulses [Eq. (15)]; parameters P and τ for the 7-core MCF with ring core configuration and modulation coefficient $M = 0.3$. The isoline $E = E_{cr} = 4\pi$ is indicated by the yellow dots; the level $H = 0$ is depicted by white dashes.

the compression point. In the area of P and τ values for which the compression occurs, the compression factor of up to 307 times can be obtained. The maximal compression is reached at the distance $z = 9.68$.

The evolution of the peak intensities in the different cores in the case of optimal combining (83.5% of all energy combines in the single core) is presented in Fig. 4. We see that the combined pulse has a smooth temporal shape with low-intensity wings. The length of combining is about 10.36 in dimensionless units, due to the slow initial development. In the final stage, as one can see in Fig. 4(a), the intensity growth

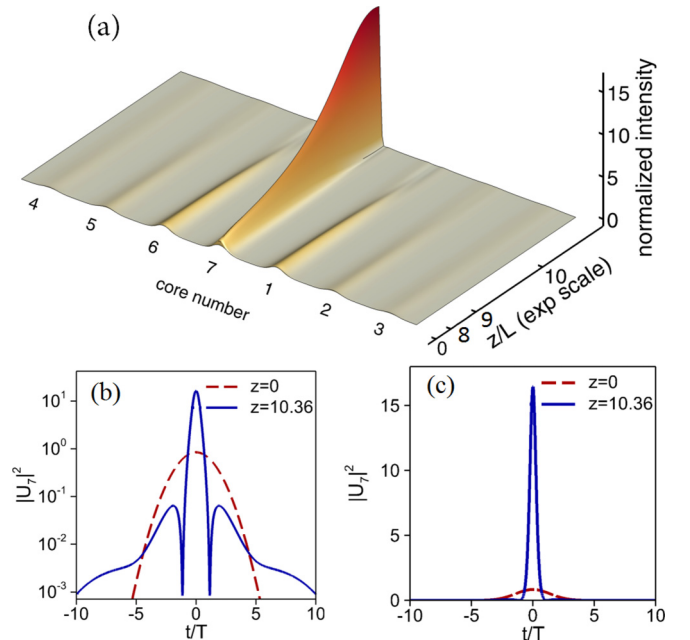


FIG. 4. Evolution of the input Gaussian pulses [Eq. (15)] with the parameters $P = 0.5$, $\tau = 2.0$, and $M = 0.3$ injected in all cores of the 7-core ring MCF (best combining) (a). Corresponding input intensity distribution in core 7 (dashed red line) and the distribution at compression point (solid blue line) are shown in logarithmic (b) and normal (c) scales. 83.5% of total input energy E is combined in core 7. The pulse width (FWHM) is reduced by 5.74x. The peak power increases in 19.5x.

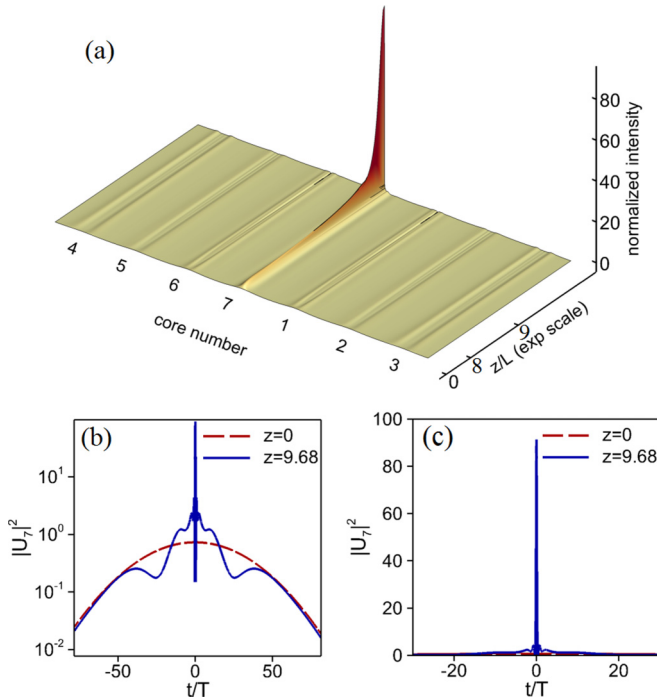


FIG. 5. Evolution of the input Gaussian pulses [Eq. (15)] with the parameters $P = 0.436$, $\tau = 42.5$, and $M = 0.3$ injected in all cores of the 7-core ring MCF (best compression) (a). Corresponding input intensity distribution in core 7 (dashed red line) and the distribution at compression point (solid blue line) are shown in logarithmic (b) and normal (c) scales. 35.8% of total input energy E is combined in the 7th core. The pulse width (FWHM) is reduced by 307.6x. The peak power increases in 123.7x.

is about exponential. The pulse compression is modest (about 6 times).

The evolution of the intensity in the different cores for the case of maximal pulse compression is presented in Fig. 5. The pulse compressed over 300 times. The compressed pulse is still mainly smooth, with noticeable wings. In this case, only about 36% of the energy combined in the compressed pulse. The interesting feature of the compression is a long initial evolution which is consistent with high sensitivity to the initial conditions.

To obtain insight for the optimal parameters for the compression and combining, let us use the continuous limit. For classical self-focusing the collapse takes place at $P > P_{cr}$. At powers well above P_{cr} , the beam breaks into filaments with a power close to P_{cr} . Using the similarity of our problem with self-focusing, we can expect that for the optimal operation the total energy $E > E_{cr}$. For $E \gg E_{cr}$ we must have the undesirable filamentation, energy concentration in a few different cores, and temporal modulations of the pulses. The results of the combining modeling are consistent with the above arguments. The parameter area where pulse compression occurs is easily distinguishable and is confined near the line $H = 0$. For optimal combining, the size of the distribution over cores and the temporal width must be comparable. As a result, we can expect that the optimal pulse duration for the combining must increase proportionally to N . The optimal combining corresponds to almost complete

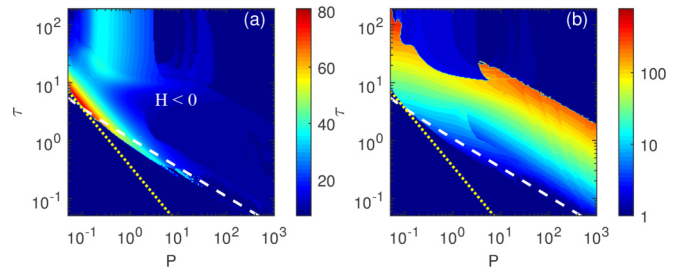


FIG. 6. Dependence of the percentage of total energy E combined in the core with pulse compression (a) and the pulse-width compression factor in the logarithmic scale (b) on the initial pulses [Eq. (15)]; parameters P and τ for the 19-core MCF with ring core configuration and modulation coefficient $M = 0.3$. The isoline $E = E_{cr} = 4\pi$ is indicated by the yellow dots; the level $H = 0$ is depicted by white dashes.

concentration in one core. The pulse compressed about 6 times, which indicates the collapse of the distribution as a whole.

To study effect of cores numbers, we compare our results with the modeling of propagation in 19-core rings. The maps of the efficiency of the combining and compression for the 19-core ring MCF are presented in Fig. 6. Qualitatively, the maps are similar to the case of 7 cores with higher sensitivity to the initial variations of the pulse energy and duration. The maximal efficiency of combining is about the same as for 7 cores and, qualitatively, the behavior is similar (see Fig. 7), but the compression distance z is much larger, namely 65.9.

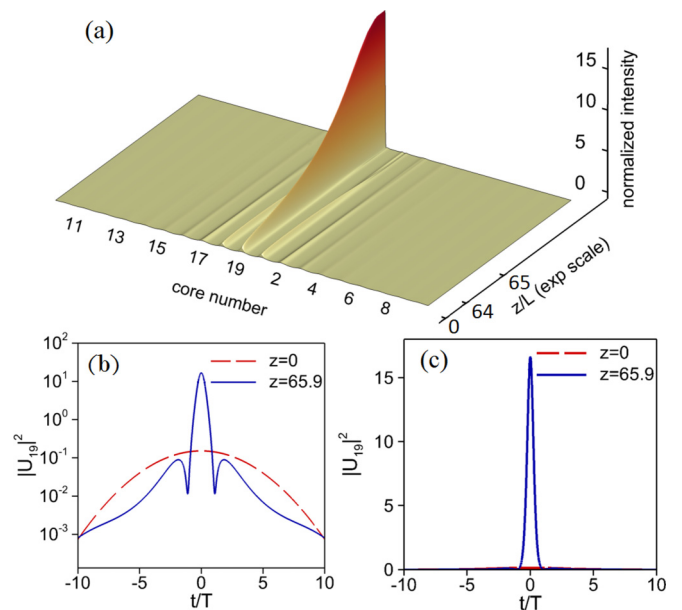


FIG. 7. Evolution of the input Gaussian pulses [Eq. (15)] with the parameters $P = 0.09$, $\tau = 4.33$, and $M = 0.3$ injected in all cores of the 19-core ring MCF (best combining) (a). The input intensity distribution in core 19 (dashed red line) and the distribution at compression point (solid blue line) are shown in logarithmic (b) and normal (c) scales. 80.0% of total input energy E is combined in the 19th core. The pulse width (FWHM) is reduced by 12.7x. The peak power increases in 111.0x.

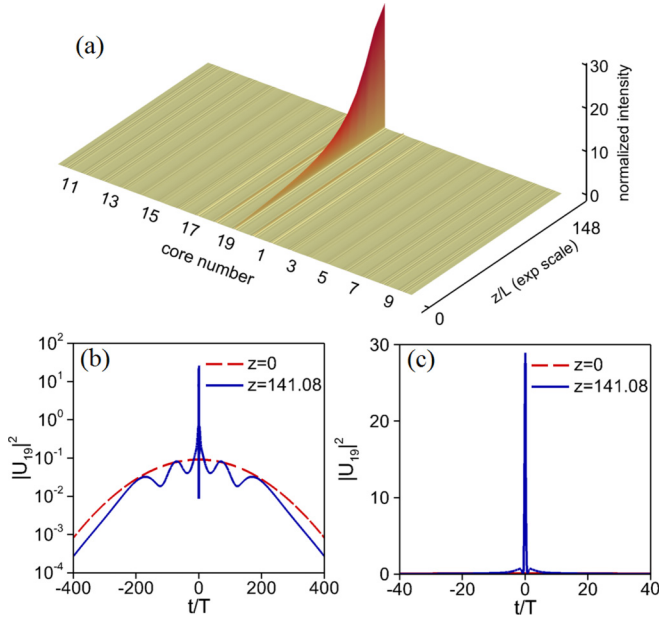


FIG. 8. Evolution of the input Gaussian pulses [Eq. (15)] with the parameters $P = 0.0545$, $\tau = 184.0$, and $M = 0.3$ injected in all cores of the 19-core ring MCF (best compression) (a). The input intensity distribution in core 19 (dashed red line) and the distribution at compression point (solid blue line) are shown in logarithmic (b) and normal (c) scales. 10.9% of total input energy E is combined in the 19th core. The pulse width (FWHM) is reduced by 720.4x. The peak power increases in 314.8x.

For the maximum combining, the compression of the pulse is higher, according to the above discussion.

The maximal compression was obtained by the initial pulses with $L_D/L_{NL} \approx 3000$ and approximately equals 720, and the compressed pulse has a smooth profile (see Fig. 8). With increase of the number of cores the optimal conditions for the maximal compression become more sensitive to the initial conditions. Also, the distance to the compression point increases and is equal to 141.08. Qualitatively, the compression and combining maps look similar (see Figs. 3–5), in agreement with continuous model arguments.

IV. COMPRESSION AND COMBINING IN HEXAGONAL AND SQUARE MCF

In this section we consider the optical MCFs with 2D core distribution design in nodes of square and hexagonal grid shown in Fig. 2. Let us start with a discussion of the continuous limit, considering the evolution of the intensity distribution according [Eq. (13)]. The collapse of the distribution in 3D (cores, coordinates, and time) takes place even for positive values of the Hamiltonian [27]. It is clear that the boundary value of $H = H_c$ corresponds to the z -independent (“stationary”) localized solution [13,23]. The distributions with $H < H_c$ collapsed.

The collapse within the 3D NLSE is weak [24], and the energy leaks from the collapse. This means that it is not beneficial to greatly increase the number of cores, and efficient combining and compression take place in the transient regime.

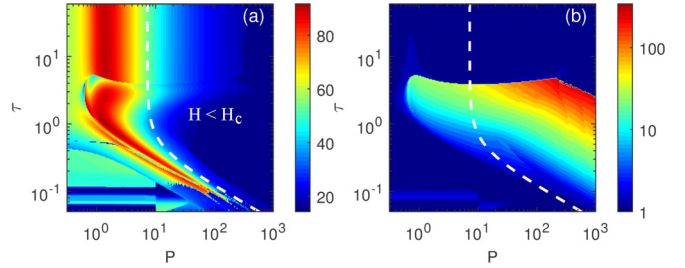


FIG. 9. Dependence of the percentage of total energy E combined in the core with pulse compression (a) and the pulse-width compression factor in the logarithmic scale (b) on the initial pulses [Eq. (15)]; parameters P and τ for the 7-core hexagonal MCF without modulation. The level $H = H_c$ is depicted by white dashes.

As was mentioned above, the initial distribution is not optimal for the collapse. The optimum for the beam combining is different from the optimum for beam compression (analog of 3D collapse).

A comprehensive analysis of pulse compression and combining in MCF with 2D location of the cores using Eqs. (6) was carried out for initial pulses having the same Gaussian profile in each core, namely,

$$U_{n,m}(z = 0, t) = \sqrt{P} \exp\left(-\frac{t^2}{2\tau^2}\right). \quad (16)$$

We compare the efficiency of a 7-core and a 19-core MCF with hexagonal core distribution and a 21-core MCF with square core configuration. Such specific core numbers are determined by the requirement of a symmetry of the hexagonal and square lattices. The dependencies of basic compression parameters are shown for the same range of parameters P , τ , as in the case of the ring MCFs.

First, we consider the hexagonal MCFs. The maps of the pulse combining and compression for 7 cores case are presented in Fig. 9. The blue area denotes pairs of parameters P and τ , for which there is no pulse compression, or the initial pulses (15) with this parameters break into filaments or are compressed after the distance along the fiber where the first local maximum of peak power is located. Due to the symmetry of the problem, both combining and compression take place in the (0,0) core. We see that the optimal conditions for combining and compression are very different from the results for the ring core distributions (Fig. 3). The optimal parameters for the compression are very different from combining similar to the ring MCF. Efficient combining takes place in a much broader range of parameters in the vertical band, insensitive to the pulse duration. This indicates that collapse takes place mainly in the transversal direction. The efficiency of combining and compression is comparable with the ring MCF, but much less sensitive to variation of the initial parameters. The maximum combining efficiency for a 7-core hexagonal MCF is better and equals 91.6% (Fig. 10) at the distance $z = 1.78$. In contrast to the ring core configurations, a wide region in the plane of parameters (P, τ) exists, where the part of the energy in the central core at the compression moment exceeds 70% of the initial energy E . The presence of this region allows us to obtain well-compressed pulses having most of the total energy E , which is of great practical importance. However, in

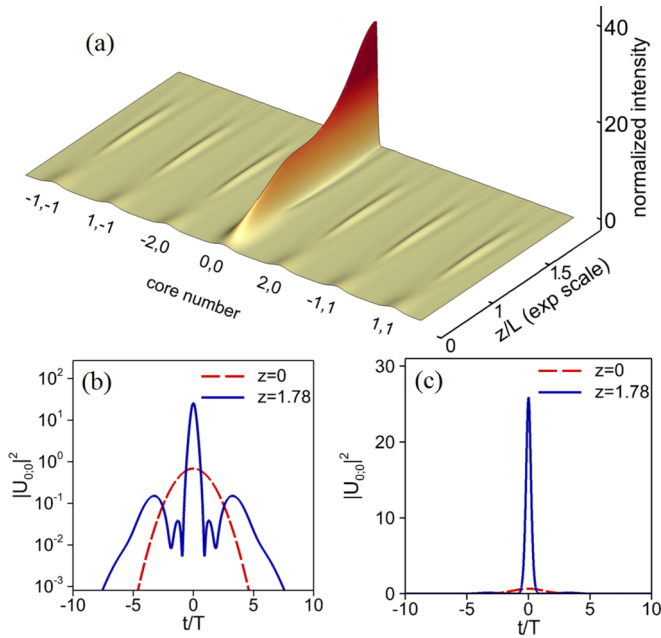


FIG. 10. Evolution of the input Gaussian pulses [Eq. (16)] with the parameters $P = 0.687$ and $\tau = 1.775$ injected in all cores of the hexagonal 7-core MCF (best combining) (a). The input intensity distribution in the central core (dashed red line) and the distribution at compression point (solid blue line) are shown in logarithmic (b) and normal (c) scales. 91.6% of total input energy E is combined in the core (0,0). The pulse width (FWHM) is reduced by 6.37x. The peak power increases in 37.7x.

this case a substantial part of the energy goes into the wings, rather than into the central peak of the compressed pulse.

An increase in the number of cores to 19 (Fig. 14) does not qualitatively change the map, and the maximal efficiency of combining is about 80.9%. Optimal combining takes place in a vertical band of parameters. The independence of the combining efficiency from the pulse duration indicates a 2D collapse in m, n variables. Another indication of the 2D nature of the combining process is that the band of the high combining efficiency is limited by the line $H = 0$, which for long pulses coincides with the 2D collapse criteria. The distance along the 19-core hexagonal fiber to the point at which the best combining occurs equals $z = 2.07$.

The distribution over cores can collapse even without pulse compression. In Figs. 9 and 12 one can see that it is possible to obtain efficient combining practically without compression. In a 2D MCF, combining and compression typically go together with different rates.

Using the 7-core fiber, a maximal pulse compression up to 256 times can be achieved (Fig. 11). In contrast to the combining pattern, at the point of maximal compression a significant fraction of energy is left in the neighbor cores. The peak power increases greatly at the compression point. The best compression occurs in the case of a high-power input pulse. Too much nonlinearity ($L_D/L_{NL} \approx 4000$) destroys the pulse shape before the compression point and confines the maximal pulse compression factor. On the other hand, it is difficult to define the optimal compression case in the presence of high nonlinearity. The pulse compression factor close to its

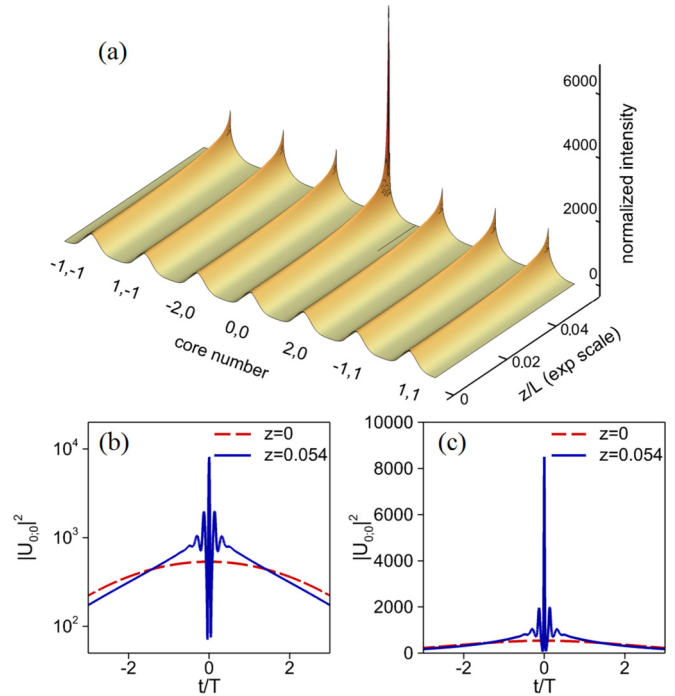


FIG. 11. Evolution of the input Gaussian pulses [Eq. (16)] with the parameters $P = 536$ and $\tau = 3.2$ injected in all cores of the hexagonal 7-core MCF (best compression) in the logarithmic scale (a). The input intensity distribution in the central core (dashed red line) and the distribution at compression point (solid blue line) are shown in logarithmic (b) and normal (c) scales. 16.6% of total input energy E is combined in the core (0,0). The pulse width (FWHM) is reduced by 256.3x. The peak power increases in 21.85x.

maximal value can be obtained for different pairs of parameters P , τ and the distance to these compression points decreases with growth of the parameter P . The compression distance is sufficiently small for both the 7-core and the 19-core hexagonal MCFs ($z \leq 0.1$ and $z \leq 0.5$, respectively).

The pulse shapes after compression and combining and the intensity evolutions are presented in Figs. 10–13. As in the ring core geometry, the compressed pulse has a smooth shape and the energy is localized mainly in one central core.

As we discussed, one can expect that the efficiency of combining and compression can degrade with increasing

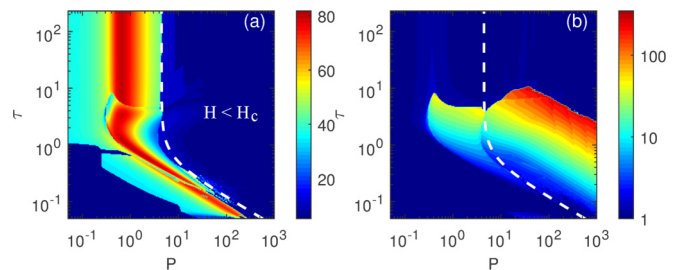


FIG. 12. Dependence of the percentage of total energy E combined in the core with pulse compression (a) and the pulse-width compression factor (b) on the initial pulses [Eq. (15)]; parameters P and τ for the 19-core hexagonal MCF without modulation. The level $H = H_c$ is depicted by white dashes.

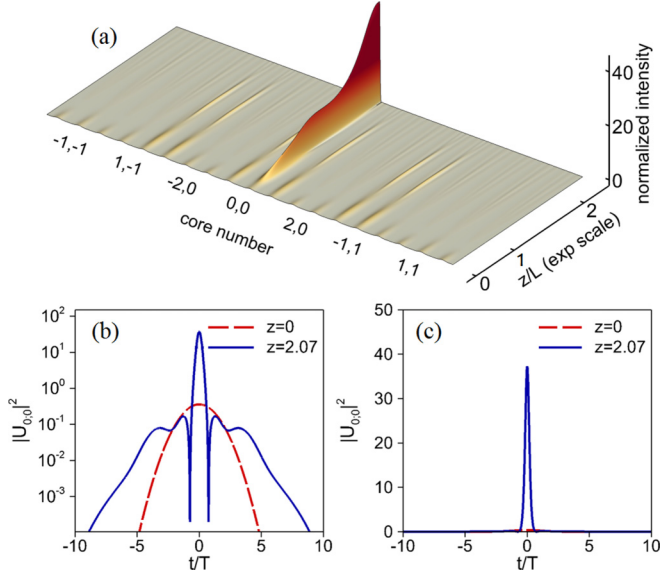


FIG. 13. Evolution of the input Gaussian pulses [Eq. (16)] with the parameters $P = 0.36$ and $\tau = 1.69$ injected in all cores of a hexagonal 19-core MCF (best combining) (a). The input intensity distribution in the central core (dashed red line) and the distribution at compression point (solid blue line) are shown in logarithmic (b) and normal (c) scale. 80.9% of total input energy E is combined in the core (0,0). The pulse width (FWHM) is reduced by 7.3x. The peak power increases in 103.4x.

numbers of cores, but the total energy in the central cores continue to grow. The stronger nonlinear interaction for a 2D MCF does not increase the efficiency of compression (combining) but greatly reduces the required distance and increases the process robustness.

Summing up, the 7-core hexagonal MCF offers a better combining than the 19-core ring MCF, but the latter one can provide higher level of compression.

Furthermore, we have tried to improve the combining scheme using a 19-core hexagonal MCF, and we have also studied its stability against modulation. First, the effect of amplitude modulation of initial pulses on compression characteristics was considered (see Fig. 14). Initial conditions were given by the same Gaussian pulses in each core, but

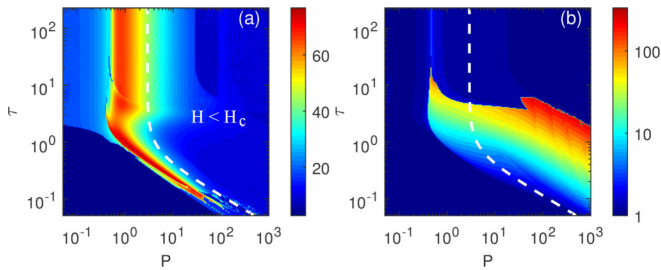


FIG. 14. Dependence of the percentage of total energy E combined in the core with pulse compression (a) and the pulse-width compression factor in the logarithmic scale (b) on the initial pulses [Eq. (17)] parameters P and τ for hexagonal 19-core MCF with modulation coefficient $M = 0.3$. The level $H = H_c$ is depicted by white dashes.

the amplitudes from core to core were slightly perturbed, depending on the distance to the central core:

$$\begin{aligned} \tilde{U}_{n,m}(0,t) &= \sqrt{P} \exp\left(-\frac{t^2}{2\tau^2}\right) \left[1 + M \cos\left(\pi \frac{n^2 + 3m^2}{N^2}\right)\right]. \end{aligned} \quad (17)$$

Here N is the maximum modulus index of a core (n or m) and M is the modulation coefficient. For calculations the value $M = 0.3$ was chosen, as in the case of ring core configurations. The influence of modulation is not as dramatic as in the case of ring MCFs, but it still has the same features. The compression region in the plane of the parameters (P, τ) is widened due to the increased robustness of the compression scheme. The absolute width of compressed pulses and pulse compression factor are less by 5%–10% as compared with the case $M = 0$, as caused by lower level of the total energy. Also the peak power increase factor lessened by up 2 times. The distance to the point of compression is less by up to 20%. The portion of the total energy E combined at the central core and at the central peak of the pulse have approximately the same order [Fig. 14(b)].

Let us now discuss the 2D core configuration with a square lattice and 21 cores. Our calculations showed that there is no noticeable difference between the square MCF and the 19-core hexagonal MCF, so we do not present figures for this type of MCF. The pulse compression factor for the hexagonal MCF is slightly smaller compared to the square MCF, and the peak power increase factor is larger for the square MCF, but these two facts can be explained by the increased number of cores ($N = 21$) and larger value of the total energy E . On the other hand, the maximum number of neighboring cores for the square MCF is less than for the hexagonal MCF (4 rather than 6), so the distance to the compression point is larger for the square MCF.

The results of all the calculations were summarized in Table I, where we added the modeling results for few more numbers of the cores. One can see that for the ring geometry, when collapse traps the fixed amount of energy, the increase in cores numbers increases the pulse compression. Because the E_{cr} is independent of core numbers the optimal conditions required the decrease of the power in the core with core number increase. It results in a decrease of the sufficient nonlinearity and increases in the length of the optimal compression and combining. The compression also becomes more sensitive to the variation of the initial pulse power and duration. For hexagonal and square core geometry the increase the number of cores does not increase the efficiency of the compression and combining, but the evolution is more robust and less sensitive to the variation of initial power and pulse durations. It is important to notice the sharp decrease in the length to the peak compression and combining points. Also, we see a small qualitative difference between the hexagonal and square geometries.

V. DISCUSSION

We have demonstrated that a MCF fiber can be effectively used for coherent wave combining and compression. The degree of compression can be continuously changed by varying the incident beam parameters. We have demonstrated the

TABLE I. Pulse parameters for maximum combining and maximum compression regimes for various types of MCFs. The unit of measurement for the distance and energy is arbitrary units, while the reduction is measured in number of times.

MCF type and number of cores	Maximum combining (%)	Distance to the maximum combining point	Energy of combined pulse	Reduction of combined pulse's duration (FWHM)	Maximum compression (FWHM)	Distance to the maximum compression point	Duration of compressed pulse
Ring 7	83.5	10.36	12.97	5.74	307.6	9.68	0.23
Ring 13	75.4	14.79	14.78	16.1	569.0	47.32	0.42
Ring 19	80.0	65.90	13.71	12.7	720.4	141.08	0.39
Square 9	91.3	3.27	12.78	6.25	≈250	<0.4	≈0.02–0.07
Square 13	82.1	2.85	14.42	6.01	≈250	<0.6	≈0.02–0.06
Square 21	80.7	3.57	16.03	5.74	≈250	<1.1	≈0.02–0.09
Hex 7	91.6	1.78	15.13	6.37	≈260	<0.1	≈0.02
Hex 13	84.7	0.99	24.44	5.00	≈250	<0.2	≈0.02–0.03
Hex 19	80.9	2.07	20.49	7.30	≈250	<0.6	≈0.02–0.07
Hex 31	75.0	1.37	43.47	5.28	≈240	<0.9	≈0.02–0.07
Hex 37	70.7	1.47	58.67	4.87	≈250	<1.3	≈0.02–0.08

possibility of compression exceeding a few hundred and coherent combining with efficiency over 80%. For a smooth distribution of energy, the evolution of the intensities in the cores is described by the NLSE: 2D for the ring core distribution and 3D for the hexagonal and square cores structures. The well-studied collapse phenomena provide insight in the processes of beam combining and compression. We have demonstrated that the combining process is consistent with collapse phenomena. However, the maximal compression regime is qualitatively different from, and the maximal compression greatly exceeds, what one can expect from the collapse model.

We have demonstrated that for the ring MCF the efficiency of compression and combining can grow with an increase in the number of cores, but the results becomes increasingly sensitive to the initial conditions. Also the length of interactions increases with the number of cores.

For a hexagonal MCF, the efficiency of combining and compressing generally degrades with increasing number of cores, but the process is more robust and insensitive to the initial conditions. Also, the interaction length is greatly reduced. This potentially makes the hexagonal MCF the best option among the considered ones for practical applications.

The above results were presented in terms of dimensionless variables, so as to be generic. Let us discuss the results in dimensional variables, choosing some specific possible applications. The typical length of interaction is a $1/C$, where C is the coupling coefficient. For a typical telecom fiber, C values for MCF $C = 15.7$ 1/km [15] and the typical length is about 64 m. The time scale $T = \sqrt{-\beta_2/(2C)}$ is about 0.8 ps. The typical scale of energy $E = CT/\gamma = 10$ pJ.

The compression of the pulses of this duration will produce within our model the pulses with few-fs duration. For such a short pulse, of course, the Kerr model of nonlinearities ceases to apply; the modification of dispersion must be taken into account. Equations (2) and (5) are not applicable anymore and the evaluation of the maximal compression required the special analysis.

If one considers MCF with weaker coupling and larger dispersion β_2 , the pulse length suitable for the compression

can be increased to the tens or hundreds of picoseconds. The compression up to 100 fs will be within our description. In this situation the wave evolution will be sensitive to the spatial variation of the coupling coefficient, and it must be evaluated before discussion of the practical applications.

Let us discuss some practical possible applications. The ultrashort pulse material processing has a multiple applications due to the small collateral damage and the absence of a heat-affected zone. To have this advantage the pulse duration must be shorter than electron-lattice exchange time, about a few picoseconds. The pulse with duration of the hundreds of picoseconds can be produced with simple electro-optic shutters. The generation of the shorter pulse required more complex and expensive technology-chirped pulse amplification. Multicore fiber compressors from hundreds to a few picoseconds can simplify the ultrashort pulse laser design and reduce their cost. The combining in MCF can be used in the fiber laser instead of amplifiers. We demonstrated that for hexagonal core patterns the efficient combining is possible practically for the all pulse durations (see Figs. 9 and 12), which can be a convenience for the laser design.

A practical device can be based on a piece of MCF. The small energy pulses injected in the different cores can be combined and compressed. It is technically difficult to make MCF with uniform coupling over the entire length (the effect of coupling spatial dependence will be discussed in the separate paper). To make a practical device, it is desirable to reduce the length of interaction. This means that one has to increase the coupling coefficient. The reduction of length to about 1 m makes it easier to keep C uniform along the MCF. In this case, the typical scale of time is 100 fs and the typical energy is about 1 nJ. We demonstrated that it is possible to combine pulses with energy $\sim 1000E_{cr} \approx 1$ μ J. By changing the parameters, it is possible to compress pulses from ps to tens of fs.

Probably, the most important point not taken into account is the spatial nonuniformity of the coupling. Technically, it is difficult to keep constant the distance between the cores in

MCFs. The coupling coefficient depends exponentially from the distance between the cores and, as a result, even for the Gaussian statistics in position variation, the coupling coefficients can be far from Gaussian. The problem is nontrivial and required special consideration.

Fortunately, the important feature of the proposed scheme is its robustness. The coupling inhomogeneity, initial phase mismatch, and delays between the pulses affect the collapse threshold only. After the collapse starts, the nonlinear effects self-organize the field evolution and make it robust.

ACKNOWLEDGMENTS

This work was supported by the Russian Science Foundation (Grant No. 14-21-00110) (work of I.S.Ch., O.V.Sh., and M.P.F.) and by the European Office of Aerospace Research and Development (Grant No. FA9550-14-1-0305) and the Grant of Ministry of Education and Science of the Russian Federation (Agreement No. 14.B25.31.0003) (work of S.K.T.). The work was partially performed under the auspices of the U.S. Department of Energy by Lawrence Livermore National Laboratory under Contract DE-AC52-07NA27344 (work of A.M.R.).

-
- [1] S. Iano, T. Sato, S. Sentsui, T. Kuroha, and Y. Nishimura, in *Optical Fiber Communication*, OSA Technical Digest Series (Optical Society of America, 1979), paper WB1.
- [2] P. J. Winzer, *IEEE Photonics Technol. Lett.* **23**, 851 (2011).
- [3] T. Morioka, Y. Awaji, R. Ryf, P. Winzer, D. Richardson, and F. Poletti, *IEEE Commun. Mag.* **50**, S31 (2012).
- [4] T. Hayashi, T. Taru, O. Shimakawa, T. Sasaki, and E. Sasaoka, *Opt. Express* **19**, 16576 (2011).
- [5] J. M. Fini, B. Zhu, T. F. Taunay, M. F. Yan, and K. S. Abedin, *Opt. Express* **20**, 949 (2012).
- [6] D. J. Richardson, J. M. Fini, and L. E. Nelson, *Nat. Photonics* **7**, 354 (2013).
- [7] R. G. H. van Uden, R. Amezcua Correa, E. Antonio Lopez, F. M. Huijskens, C. Xia, G. Li, A. Schülzgen, H. de Waardt, A. M. J. Koonen, and C. M. Okonkwo, *Nat. Photonics* **8**, 865 (2014).
- [8] K. Igarashi, T. Tsuntani, and I. Morita, in *Optical Communication (ECOC)* (Systematic Paris Region Systems and ICT Cluster, 2014), pp. 1–3.
- [9] T. A. Eriksson, R. S. Luís, B. J. Puttnam, J. M. D. Mendinueta, P. A. Andrekson, M. Karlsson, Y. Awaji, N. Wada, and E. Agrell, *Opt. Express* **23**, 14569 (2015).
- [10] K. Saitoh and S. Matsuo, *J. Lightwave Technol.* **34**, 55 (2016).
- [11] D. J. Richardson, J. Nilsson, and W. A. Clarkson, *J. Opt. Soc. Am. B* **27**, B63 (2010).
- [12] Y. S. Kivshar and G. P. Agrawal, *Optical Solitons: From Fibers to Photonic Crystals*, 5th ed. (Academic Press, New York, 2003).
- [13] S. K. Turitsyn, A. M. Rubenchik, M. P. Fedoruk, and E. Tkachenko, *Phys. Rev. A* **86**, 031804 (2012).
- [14] C. Agger, S. T. Sørensen, C. L. Thomsen, S. R. Keiding, and O. Bang, *Opt. Lett.* **36**, 2596 (2011).
- [15] S. Mumtaz, R. Essiambre, and G. Agrawal, *IEEE Photonics Technol. Lett.* **24**, 1574 (2012).
- [16] A. B. Aceves, G. G. Luther, C. De Angelis, A. M. Rubenchik, and S. K. Turitsyn, *Phys. Rev. Lett.* **75**, 73 (1995).
- [17] T. Fan, *IEEE J. Sel. Top. Quantum Electron.* **11**, 567 (2005).
- [18] V. E. Zakharov and E. A. Kuznetsov, *Phys. Usp.* **55**, 535 (2012).
- [19] A. M. Rubenchik, I. S. Chekhovskoy, M. P. Fedoruk, O. V. Shtyrina, and S. K. Turitsyn, *Opt. Lett.* **40**, 721 (2015).
- [20] S. Mumtaz, R. Essiambre, and G. Agrawal, *J. Lightwave Technol.* **31**, 398 (2013).
- [21] S. Mumtaz, G. P. Agrawal, and R.-J. Essiambre, in *Frontiers in Optics 2012/Laser Science XXVIII* (Optical Society of America, Washington, DC, 2012), p. FW1D.2.
- [22] A. B. Aceves, O. V. Shtyrina, A. M. Rubenchik, M. P. Fedoruk, and S. K. Turitsyn, *Phys. Rev. A* **91**, 033810 (2015).
- [23] E. A. Kuznetsov, J. J. Rasmussen, K. Rypdal, and S. K. Turitsyn, *Phys. D (Amsterdam, Neth.)* **87**, 273 (1995).
- [24] S. K. Turitsyn, B. G. Bale, and M. P. Fedoruk, *Phys. Rep.* **521**, 135 (2012).
- [25] N. Higham, *SIAM J. Matrix Anal. Appl.* **26**, 1179 (2005).
- [26] K. Hizanidis, S. Droulias, I. Tsopelas, N. K. Efremidis, and D. N. Christodoulides, *Int. J. Bifurcation Chaos* **16**, 1739 (2006).
- [27] S. K. Turitsyn, *Phys. Rev. E* **47**, R13 (1993).